# High-Efficiency Asymmetrical Half-Bridge Converter With Linear Voltage Gain

Juhyun Bae, *Student Member, IEEE*, Jae-Sang Kim, *Student Member, IEEE*, Minsu Lee, *Student Member, IEEE*, Jung-Kyu Han, *Member, IEEE*, and Gun-Woo Moon, *Member, IEEE*

***Abstract*—A conventional asymmetrical half-bridge (AHB) converter is one of the widely used topologies in low to medium power applications. However, when it is designed in a wide input voltage range, it operates with a low duty ratio at nominal input voltage. In addition, it has disadvantages, such as a dc offset of magnetizing current, an unbalanced average current of the diode, and a nonlinear voltage gain due to asymmetrical operation. To solve these disadvantages, an AHB converter with linear voltage gain is proposed. The proposed converter has a structure in which a capacitor is added as a voltage source to obtain a symmetrical operation by extending the commutation period. Therefore, it has a narrow range of operating duty ratio and a zero dc offset of magnetizing current. Due to the zero dc offset of magnetizing current, it has a small size transformer and improved zero-voltage switching conditions of the primary-side switches. In addition, it has a low primary rms current and a balanced average current of the diode. Consequently, the proposed converter has high efficiency under the entire load conditions. A 300–400 V input and 48 V/400 W output prototype is tested to verify the feasibility of the proposed converter.**

***Index Terms*—Asymmetrical half-bridge (AHB) converter, dc offset of magnetizing current, high efficiency, linear voltage gain.**

## I. Introduction

With the recent advent of smart factories, industrial automation, such as industrial robots and machine vision, has been developing. Accordingly, power consumption as well as the market size of automated industrial machines is continuously increasing. In line with this trend, research on industrial power supplies has been conducted. There are two considerations in designing an industrial power supply. First, automated industrial machines are changing to 48 V systems instead of 12 V systems for high efficiency and high density. Second, the power supply should be designed to satisfy the hold-up condition, which maintains the output voltage for a certain time after the loss of the ac line voltage. Therefore, many studies have been conducted on 48 V power supplies with high efficiency under a wide input voltage range [1], [2].

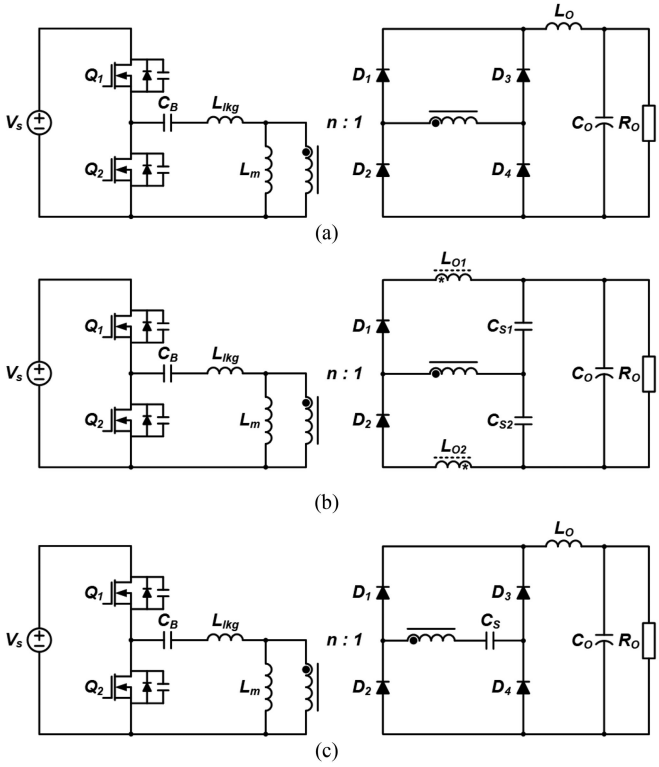


Fig. 1. Circuit diagrams of various AHB converters. (a) Conventional AHB converter. (b) AHB converter with the CIR. (c) Proposed converter.

An asymmetrical half-bridge (AHB) converter, as shown in Fig. 1(a), is one of the popular topologies in low to medium power applications due to its small number of elements, inherent zero-voltage switching (ZVS) capability, and simple pulse width modulation (PWM) control [3]–[8]. However, a conventional AHB converter has the following disadvantages when it is designed in a wide input voltage range to satisfy a hold-up condition. The first disadvantage is the dc offset of magnetizing current in the transformer. As shown in Fig. 2(a), the dc offset of magnetizing current not only increases the size of the transformer but also worsens the ZVS condition of switch $Q_1$ [9]. To achieve the ZVS of $Q_1$, magnetizing inductance $L_m$ should be small. As a result, the conventional AHB converter has a

Manuscript received 24 January 2022; revised 28 April 2022; accepted 1 June 2022. Date of publication 15 June 2022; date of current version 6 September 2022. This work was supported by the National Research Foundation of Korea Grant funded by the Korea Government (MSIP) under Grant 2019R1A2B5B02070509. Recommended for publication by Associate Editor J. Lam. *(Corresponding author: Gun-Woo Moon.)*

Juhyun Bae, Jae-Sang Kim, Minsu Lee, and Gun-Woo Moon are with the Department of Electrical Engineering, Korea Advanced Institute of Science and Technology, Daejeon 34141, South Korea (e-mail: wngus7158@kaist.ac.kr; jaesangkim@kaist.ac.kr; trevin6248@kaist.ac.kr; gwmoon@kaist.ac.kr).

Jung-Kyu Han is with the Department of Electronics and Control Engineering, Hanbat National University, Daejeon 305-719, South Korea (e-mail: hanjk715@gmail.com).

Color versions of one or more figures in this article are available at https://doi.org/10.1109/TPEL.2022.3183260.

Digital Object Identifier 10.1109/TPEL.2022.3183260

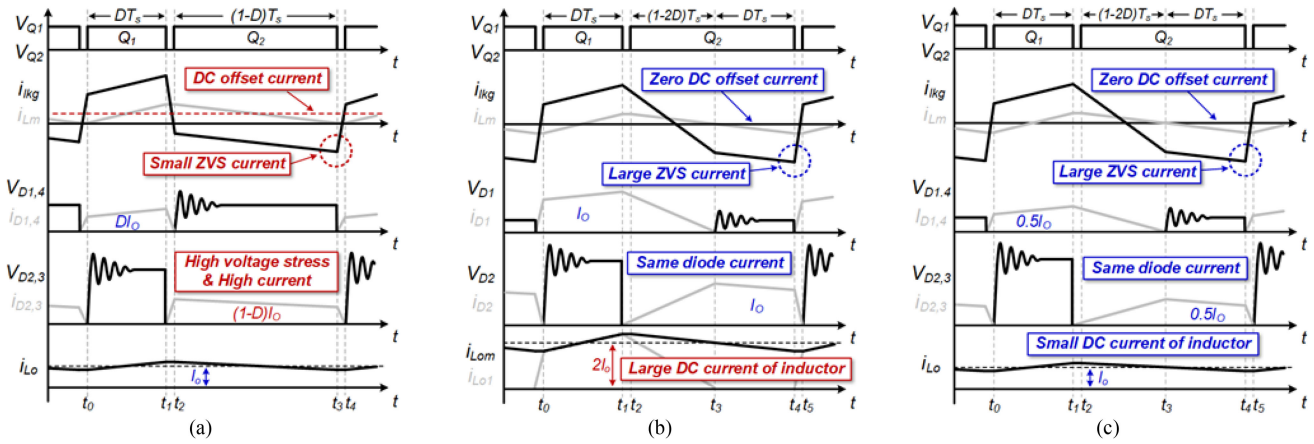


Fig. 2. Key waveforms of various AHB converters. (a) Conventional AHB converter. (b) AHB converter with the CIR. (c) Proposed converter.

high primary rms current, and it causes a large conduction loss of the transformer. The second disadvantage is an unbalanced average current of the diode. A high average current flows through diodes with high voltage stress that have a high forward voltage drop $V_F$. As a result, it causes a large conduction loss of diode. The third disadvantage is nonlinear voltage gain. For the same input voltage range, the conventional AHB converter has a wider range of operating duty ratio compared with the converter with a linear voltage gain. In addition, it operates with a lower duty ratio beyond the optimum operating point at the nominal input voltage. Therefore, the dc offset of magnetizing current increases, and the voltage and current stress of the rectifier diode become even more asymmetrical [10]–[13].

To overcome the drawbacks of the conventional AHB converter, several studies have been conducted [14]–[21]. Among them, an AHB converter with duty-cycle-shifted PWM control was proposed in [18]. It has a linear voltage gain and zero dc offset of magnetizing current through symmetrical powering. Hence, the ZVS condition of $Q_1$ is improved. However, the use of an additional auxiliary switch and diode increases cost and complexity. In addition, high freewheeling current conducts in the additional components, and it causes large conduction loss of the primary side.

Recently, a representative paper that effectively solves many shortcomings of the conventional AHB converter was proposed in [21]. As shown in Fig. 1(b), an AHB converter with a coupled inductor rectifier (CIR) has a structure in which a coupled inductor is added to the voltage doubler rectifier. According to the coupled inductor and the secondary-side doubler capacitors $C_{S1}$ and $C_{S2}$, it obtains an extended commutation period, as shown in Fig. 2(b). As a result, it has a linear voltage gain and symmetrical operation. By linear voltage gain, it operates with a higher duty ratio than the conventional AHB converter at nominal input voltage. In addition, the dc offset of magnetizing current is eliminated by $C_{S1}$ and $C_{S2}$. Due to the zero dc offset of magnetizing current, the AHB converter with the CIR has the improved ZVS condition of $Q_1$. Therefore, it has a low primary rms current by large $L_m$. Moreover, the average current of all rectifier diodes is the output current $I_O$. Since a balanced average current of diodes flows regardless of the voltage stress of the diode, it has a small conduction loss. However, the offset current of the coupled inductor becomes twice the $I_O$. As a result, it has a high rms current of the coupled inductor, and it causes large conduction loss. Thus, the AHB converter with the CIR is not suitable for high output current applications because of its low efficiency under heavy-load conditions.

It is necessary to study a circuit that not only has a linear voltage gain and symmetrical operation but also has high efficiency under entire load conditions. In this article, an AHB converter with linear voltage gain is proposed to achieve high efficiency under heavy-load conditions as well as light-load conditions. As shown in Fig. 1(c), the proposed converter has a structure in which one capacitor is added in series to a full-bridge rectifier. According to the secondary capacitor $C_S$, it obtains an extended commutation period, as shown in Fig. 2(c). As a result, it has a linear voltage gain and symmetrical operation. In addition, the dc offset of magnetizing current is eliminated by $C_S$. The advantages of the proposed converter are as follows.

1) Due to linear voltage gain, it can be designed with a narrower range of operating duty ratio than the conventional AHB converter. Thus, it operates with a higher duty ratio at nominal input voltage.
2) Due to zero dc offset of magnetizing current, it has the improved ZVS condition of $Q_1$. Thus, it has a small switching loss under light-load conditions.
3) Due to large $L_m$, it has a low primary rms current. Thus, it has a small conduction loss of the transformer.
4) Due to a balanced average current $0.5I_O$ of all rectifier diodes, it has a small conduction loss. In addition, lower current-rating diodes with good reverse recovery characteristics can be used.

Because of the above advantages, it achieves higher efficiency under entire load conditions than the aforementioned AHB converters.

The rest of this article is organized as follows. The derivation and operational principles are focused on Sections II and III, respectively. In Section IV, the characteristics and design considerations of the proposed converter are analyzed. A 300–400 V

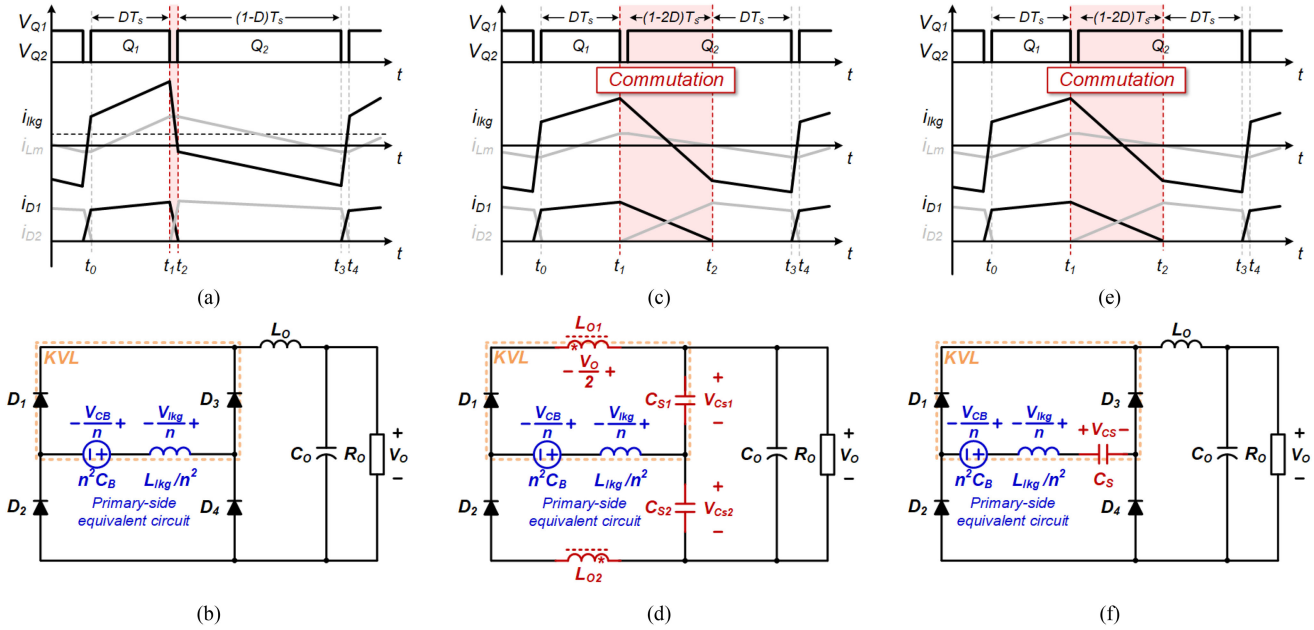


Fig. 3. Key waveforms and secondary-side equivalent circuit. (a) and (b) Conventional AHB converter. (c) and (d) AHB converter with the CIR. (e) and (f) Proposed converter.

input and 48 V/400 W output laboratory prototype operating at 100 kHz is built and tested to verify the effectiveness of the proposed converter in Section V. Finally, Section VI concludes this article.

## II. Derivation of the Proposed Converter

This section compares and analyzes the conventional AHB converter and the AHB converter with the CIR [21]. Besides, it introduces how the proposed converter is derived. In general, a half-bridge converter with an output inductor $L_O$ can be divided into three intervals, as shown in Fig. 3. Positive powering interval is a period $[t_0\text{-}t_1]$ for powering with $I_o/n$, negative powering interval is a period $[t_2\text{-}t_3]$ for powering with $-I_o/n$, and commutation interval is a period$[t_1\text{-}t_2]$ in which all rectifier diodes conduct.

In the case of the conventional AHB converter, as shown in Fig. 3(a), the period$[t_0\text{-}t_1]$ for positive powering and the period$[t_2\text{-}t_3]$ for negative powering are asymmetrical. Therefore, the dc offset of magnetizing current is generated to achieve the current-second balance of the primary blocking capacitor $C_B$. Fig. 3(b) shows a secondary-side equivalent circuit of the conventional AHB converter during the commutation period. Since it is a commutation period, all rectifier diodes conduct. Kirchhoff's voltage law (KVL) is applied to the yellow dotted loop as follows:

$$\frac{v_{lkg}}{n}+\frac{V_{CB}}{n}+v_{D3}-v_{D1}=0 \tag{1}$$

where $v_{lkg}$ is the voltage across a leakage inductor $L_{lkg}$, $V_{CB}$ is the voltage of a blocking capacitor, $n$ is the turn ratio of the transformer, $v_{D1}$ is the voltage stress of diode $D_1$, $v_{D3}$ is the voltage stress of diode $D_3$, and $v_{D1}=v_{D3}=0$ during commutation period. Meanwhile, a large $V_{CB}$ is applied to $v_{lkg}$. As a result, the primary current $i_{lkg}$ has a steep slope, and the period$[t_1\text{-}t_2]$ for the commutation period is shortened, as shown in Fig. 3(a).

In the case of the AHB converter with the CIR, as shown in Fig. 3(c), the period$[t_0\text{-}t_1]$ for positive powering and the period$[t_2\text{-}t_3]$ for negative powering are symmetrical by the extended commutation period$[t_1\text{-}t_2]$. Thus, there is no dc offset of magnetizing current. Fig. 3(d) shows a secondary-side equivalent circuit of the AHB converter with the CIR during the commutation period. All rectifier diodes conduct, and half of the output voltage is applied to the coupled inductor. Since the output voltage is $2DV_S/n$, the voltage across coupled inductor $v_{Lo}$ is $DV_S/n$. In the same way, KVL is applied to the yellow dotted loop as follows:

$$\frac{v_{lkg}}{n}+\frac{V_{CB}}{n}-\frac{V_O}{2}+V_{CS1}-v_{D1}=0 \tag{2}$$

where $v_{D1}=0$ during the commutation period. At this time, the voltage of secondary capacitors $V_{Cs1}$ and $V_{Cs2}$ can be obtained using the slope equation of the $i_{lkg}$ during the dead time [21].

$$V_{CS1}=\frac{4I_OL_{lkg}}{n^2(1-2D)T_S} \tag{3}$$

$$V_{CS2}=V_O-\frac{4I_OL_{lkg}}{n^2(1-2D)T_S}. \tag{4}$$

Because $V_{CB}/n$ is the same as $v_{Lo}$, and they cancel out each other through (2). Therefore, $nV_{CS1}$ is applied to $v_{lkg}$, and $V_{CS1}$ becomes very small at nominal input voltage. As a result, $i_{lkg}$ has a gentle slope, and the commutation period$[t_1\text{-}t_2]$ is extended for symmetrical operation, as shown in Fig. 3(c).

However, the AHB converter with the CIR has a disadvantage in which large conduction loss occurs due to the coupled inductor. Meanwhile, the proposed converter has the same advantages

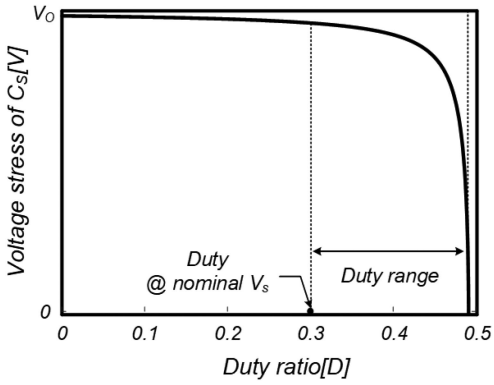


Fig. 4. Voltage stress of $C_S$.

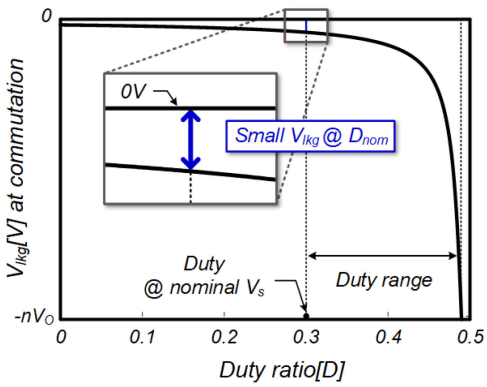


Fig. 5. $V_{lkg}$ at commutation period.

as the AHB converter with the CIR through symmetrical operation and solves the disadvantages caused by the coupled inductor presented in [21]. To obtain the extended commutation period, a voltage source that can reduce a large $v_{lkg}$ during the commutation period is required. Therefore, the proposed converter has a structure in which one capacitor is added to the secondary side as the voltage source. Fig. 3(f) shows a secondary-side equivalent circuit of the proposed converter during the commutation period. Since it is a commutation period, all rectifier diodes conduct. KVL is applied to the yellow dotted loop as follows:

$$\frac{v_{lkg}}{n}+\frac{V_{CB}}{n}-V_{CS}+v_{D3}-v_{D1}=0 \tag{5}$$

where $v_{D1}=v_{D3}=0$ during the commutation period. At this time, the voltage of secondary capacitor $V_{CS}$ can be obtained using the slope equation of $i_{lkg}$ (6) during the dead time.

$$\frac{-V_{CB}+nV_{CS}}{L_{lkg}}\cdot(1-2D)T_S=\frac{2I_O}{n} \tag{6}$$

$$V_{CS}=V_O-\frac{2I_OL_{lkg}}{n^2(1-2D)T_S}. \tag{7}$$

Using (5), $nV_{CS}-V_{CB}$ is applied to $v_{lkg}$ as follows:

$$v_{lkg}=nV_{CS}-V_O=-\frac{2I_OL_{lkg}}{n(1-2D)T_S}=-\frac{2I_OL_{lkg}}{n(1-2\frac{nV_O}{V_S})T_S}. \tag{8}$$

As $V_{CB}/n$ is almost similar to $V_{CS}$ at nominal input voltage through (7) and Fig. 4, they almost cancel out each other. Therefore, $v_{lkg}$, as shown in Fig. 5, becomes very small at a nominal input voltage. As a result, $i_{lkg}$ has a gentle slope, and the commutation period[$t_1$-$t_2$] is extended for symmetrical operation, as shown in Fig. 3(e).

When the input voltage decreases or the output current increases, the operating duty ratio increases. As shown in Fig. 5, as the operating duty ratio increases, the absolute value of $v_{lkg}$ at the commutation period also increases. As a result, the commutation period [$t_1$-$t_2$] is shortened and symmetrical operation can be maintained. Therefore, since the $v_{lkg}$ at the commutation period changes according to the change of the input voltage and the output current to maintain a symmetrical operation, the commutation period [$t_1$-$t_2$] is shorter than $(1-D)T_S$.

Consequently, the proposed converter not only has a low rms current of $L_O$ because the offset current of $L_O$ is $I_O$ but also can achieve high efficiency due to its symmetrical operation.

## III. Operational Principles

Figs. 6 and 7 show the operating modes and key waveforms of the proposed converter, respectively. The primary-side configuration and control method are the same as that of the conventional AHB converter. Accordingly, the proposed converter has five operation modes, as shown in Fig. 7. To simplify the analysis of operation, several assumptions are made as follows.

1) $C_B$ and $C_S$ are large enough to be considered as constant voltage sources.
2) The primary switches $Q_1$ and $Q_2$ are ideal except for internal diodes $D_{s1}$ and $D_{s2}$ and output capacitors $C_{oss1}$ and $C_{oss2}$.
3) Rectifier diodes $D_1$ and $D_2$ are ideal except for junction capacitors $C_{j1}$ and $C_{j2}$.

*Mode 1* [$t_0$-$t_1$]*:* Mode 1 starts when $Q_1$ is turned ON. $Q_1$ is turned ON with the ZVS because $C_{oss1}$ is all discharged in Mode 5. In this mode, a voltage across magnetizing inductor $v_{Lm}$ is the difference between an input voltage $V_S$ and $V_{CB}$. Therefore, $V_S-V_{CB}$ is transferred to the secondary side and powered to the output through $D_1$, $D_4$, and $C_S$. Furthermore, a voltage across output inductor $v_{Lo}$ is $(V_S-V_{CB})/n+V_{CS}-V_o$. In addition, voltages of $D_2$ and $D_3$ are $2\{(V_S-V_{CB})/n+V_{CS}\}$ considering the resonance of $C_{j1}$, $C_{j2}$, and $L_{lkg}$.

*Mode 2* [$t_1$-$t_2$]*:* Mode 2 starts when $Q_1$ is turned OFF. In this mode, $i_{lkg}$ charges and discharges $C_{oss1}$ and $C_{oss2}$, respectively. When a transformer secondary-side voltage $v_{rec}$ decreases to $-V_{CS}$, $D_2$ and $D_3$ conduct. Accordingly, all rectifier diodes conduct, and a commutation occurs. At this time, $v_{rec}$ is clamped to $-V_{CS}$, and $v_{Lm}$ becomes $-nV_{CS}$. As a result, a small voltage of $nV_{CS}-V_{CB}$ is applied to $v_{lkg}$, and $i_{lkg}$ has a gentle slope of $(nV_{CS}-V_{CB})/L_{lkg}$.

*Mode 3* [$t_2$-$t_3$]*:* Mode 3 starts when $Q_2$ is turned ON. $Q_2$ is turned ON with the ZVS because $C_{oss2}$ is all discharged in Mode 2. In Mode 3, the commutation period continues as in Mode 2, and $i_{lkg}$ is decreased with the same slope.

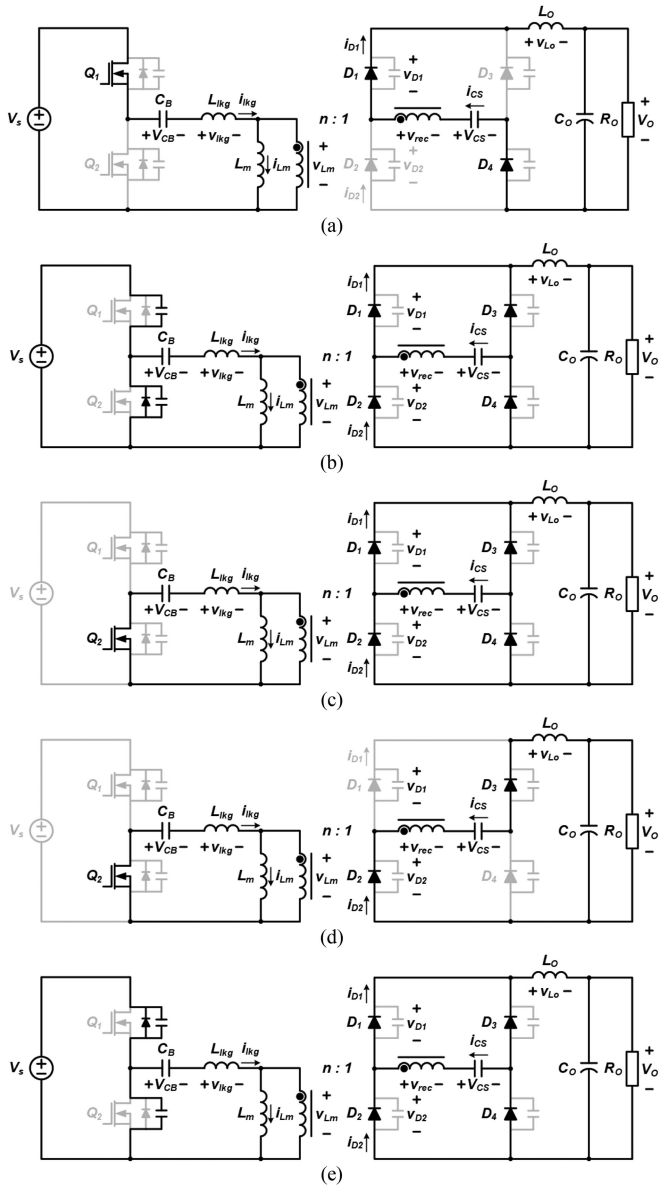


Fig. 6. Current path of the proposed converter. (a) Mode 1. (b) Mode 2. (c) Mode 3. (d) Mode 4. (e) Mode 5.

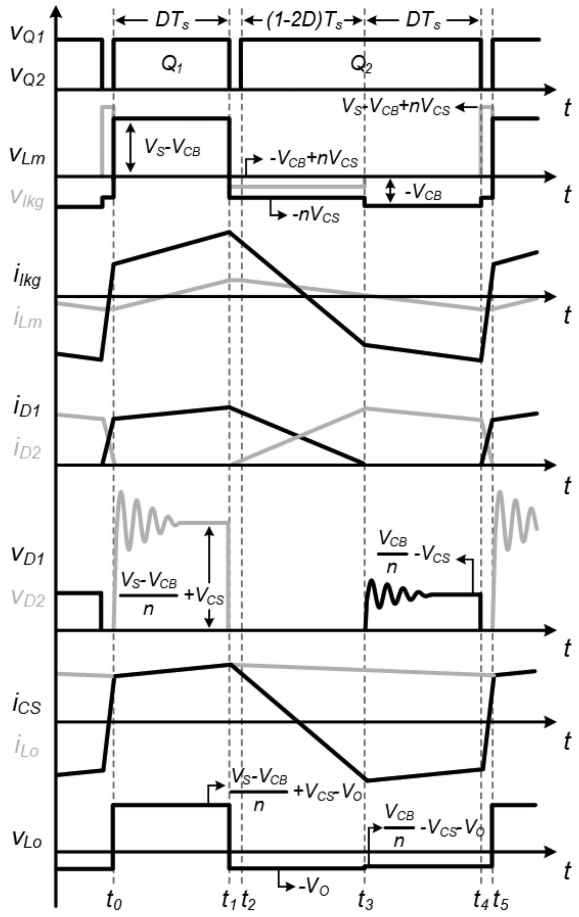


Fig. 7. Key waveforms of the proposed converter.

TABLE I
SPECIFICATIONS OF PROTOTYPE CONVERTERS

| | *Parameters* |
|---|---|
| Input voltage, $V_S$ | 300 – 400 V |
| Output voltage, $V_O$ | 48 V |
| Output power, $P_O$ | 400 W |
| Switching frequency, $f_s$ | 100 kHz |

*Mode 4* [$t_3$-$t_4$]*:* Mode 4 starts at the end of the commutation period. In this mode, $v_{Lm}$ is $-V_{CB}$. Therefore, $-V_{CB}$ is transferred to the secondary side and powered to the output through $D_2$, $D_3$, and $C_S$. Furthermore, $v_{Lo}$ is $V_{CB}/n-V_{CS}-V_o$. In addition, voltages of $D_1$ and $D_4$ are $2(V_{CB}/n-V_{CS})$, considering the resonance of $C_{j1}$, $C_{j2}$, and $L_{lkg}$.

*Mode 5* [$t_4$-$t_5$]*:* Mode 5 starts when $Q_2$ is turned OFF. In this mode, $i_{lkg}$ discharges and charges $C_{oss1}$ and $C_{oss2}$, respectively. When $v_{rec}$ increases to $-V_{CS}$, $D_1$ and $D_4$ conduct. Accordingly, all rectifier diodes conduct, and the commutation occurs. At this time, $v_{rec}$ is clamped to $-V_{CS}$, and $v_{Lm}$ becomes $-nV_{CS}$. As a result, unlike mode 2, a large voltage of $V_S-V_{CB}+nV_{CS}$ is applied to $v_{lkg}$, and $i_{lkg}$ has a steep slope of $(V_S-V_{CB}+nV_{CS})/L_{lkg}$.

## IV. CHARACTERISTICS AND DESIGN CONSIDERATIONS OF THE PROPOSED CONVERTER

To illustrate the design procedure of the proposed converter, a specification for industrial power supply in Table I is used in this section. The characteristics and design procedure of the proposed converter are as follows.

### A. Voltage Gain

The voltage gain of the proposed converter is linear that differs from the conventional AHB converter, and it can be obtained by the voltage-second balance of $L_o$ and $L_m$. To ease the complexity of analysis, it is assumed that the dead time is small enough to be neglected. The voltage-second balance is applied to $L_o$ and

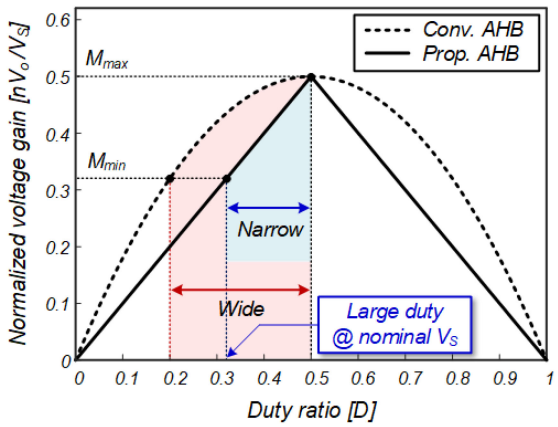


Fig. 8. Normalized voltage gain.

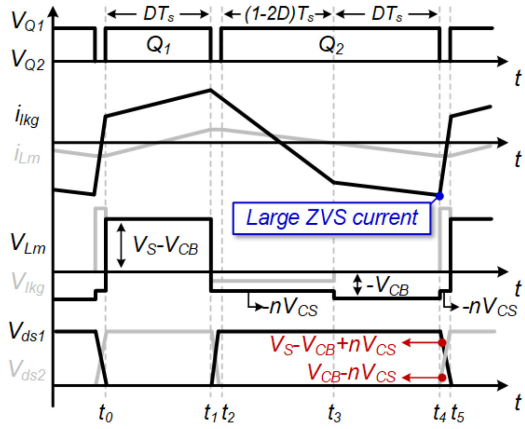


Fig. 9. ZVS waveforms of the proposed converter.

$L_m$ as follows:

$$D\left(\frac{V_S - V_{CB}}{n} + V_{CS} - V_O\right) - (1-2D)V_O + D\left(\frac{V_{CB}}{n} - V_{CS} - V_O\right) = 0 \quad (9)$$

$$D(V_S - V_{CB}) + (1-2D)(-nV_{CS}) + D(-V_{CB}) = 0. \quad (10)$$

From (9) and (10), $V_{CB}$ and voltage gain are, respectively, obtained as follows:

$$V_{CB} = DV_S \quad (11)$$

$$G_v = \frac{V_O}{V_S} = \frac{D}{n}. \quad (12)$$

Normalized voltage gain graphs of the conventional AHB converter and the proposed converter are shown in Fig. 8. The operating duty ratio of the conventional AHB converter is designed to be 0.2 to 0.5 due to the nonlinear voltage gain. Therefore, it operates with a lower duty ratio at nominal input voltage, resulting in greater asymmetry. However, since the proposed converter has linear voltage gain, the operating duty ratio is designed to be 0.32 to 0.5, which is a relatively narrow range. As a result, it has a relatively high operating duty ratio at nominal input voltage.

Moreover, the conventional AHB converter and the proposed converter have the same maximum voltage gain at a duty ratio of 0.5 in an ideal case. In practice, the proposed converter has a relatively large effective gain due to its small duty loss. Accordingly, if the turn ratio is selected to provide the output of 48 V in a given input voltage range, it is as follows. The turn ratio of the conventional AHB converter is designed as 2.31. On the other hand, the turn ratios of the AHB converter with CIR and the proposed converter are designed as 5.1 and 2.55, respectively.

### B. DC Offset of Magnetizing Current in the Transformer

The dc offset of magnetizing current can be obtained by the following equation:

$$< i_{lkg} > = < i_{Lm} > + \frac{< i_{\sec} >}{n} \quad (13)$$

where $<i_{lkg}>$ is the average current of the primary side, $<i_{Lm}>$ is the average current of the magnetizing inductor, and $<i_{\sec}>$ is the average current of the secondary side.

By the charge balance of the capacitor, the average current flowing through the capacitor during one cycle becomes zero. Therefore, $<i_{lkg}>$ is zero by $C_B$. As a result, from (13), the dc offset of magnetizing current is the average current flowing from the secondary side to the primary side.

In the case of the conventional AHB converter, when $Q_1$ is turned ON during $DT_s$, it powers through $D_1$ and $D_4$. However, when $Q_2$ is turned ON during $(1-D)T_s$, it powers through $D_2$ and $D_3$. Thus, $<i_{\sec}>$ during $DT_s$ and $(1-D)T_s$ is $DI_o$ and $(1-D)I_o$, respectively. As a result, the conventional AHB converter has the dc offset of magnetizing current of $(1-2D)I_o/n$. As the input voltage range is wide, it operates with a lower duty ratio at nominal input voltage. Therefore, it has a large dc offset of magnetizing current, and it limits the use of the maximum magnetic flux density, which increases the size of the transformer.

Meanwhile, in the case of the AHB converter with the CIR and the proposed converter, $<i_{\sec}>$ becomes zero by the charge balance of the secondary capacitor. As a result, the AHB converter with the CIR and the proposed converter have a zero dc offset of magnetizing current regardless of duty ratio and can be designed as a small size transformer.

### C. ZVS Conditions

As shown in Fig. 9, when the commutation period starts, $v_{rec}$ and $v_{Lm}$ are clamped to $-V_{CS}$ and $-nV_{CS}$, respectively. At this time, $C_{oss1}$ and $C_{oss2}$ are charged and discharged by $i_{lkg}$. Based on Fig. 9, the ZVS conditions of $Q_1$ and $Q_2$ in the proposed converter are obtained as follows:

$$\frac{1}{2}L_{lkg}\left(-\frac{I_O}{n} - \frac{v_{Lm}}{2L_m}DT_S\right)^2 \geq \frac{1}{2}C_{oss}V_S^2 - \frac{1}{2}C_{oss}(V_{CB}-nV_{CS})^2 + \frac{1}{2}C_{oss}(V_S - V_{CB} + nV_{CS})^2 = C_{oss}\left(V_S^2 - \frac{2V_S I_O L_{lkg}}{n(1-2D)T_S}\right) \quad (14)$$

$$\frac{1}{2}L_{lkg}\left(\frac{I_O}{n} + \frac{v_{Lm}}{2L_m}DT_S\right)^2$$

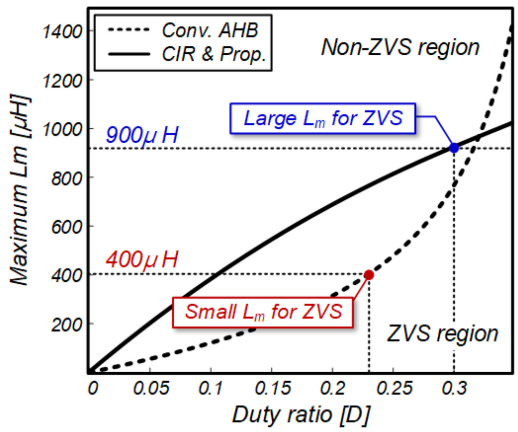


Fig. 10. Required $L_m$ for ZVS of $Q_1$ under 50% load conditions.

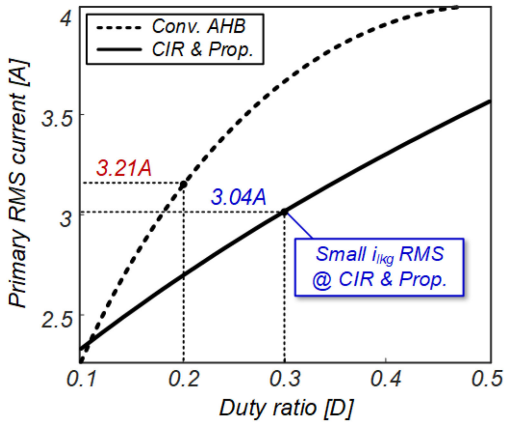


Fig. 11. Comparison of primary rms current.

$$\geq \frac{1}{2}C_{oss}(V_{CB}-nV_{CS})^2+\frac{1}{2}C_{oss}V_S^2-\frac{1}{2}C_{oss}(V_S-V_{CB}+nV_{CS})^2$$
$$= C_{oss}\left(\frac{2V_SI_OL_{lkg}}{n(1-2D)T_S}\right). \quad (15)$$

Since the required ZVS energy of $Q_1$ is greater than that of $Q_2$, $L_m$ and $L_{lkg}$ are designed to satisfy the ZVS condition of $Q_1$.

In case of the conventional AHB converter, the dc offset of magnetizing current worsens the ZVS condition of $Q_1$. Meanwhile, the AHB converter with CIR and the proposed converter do not have asymmetry of primary current since magnetizing current does not have dc offset. Therefore, they have a large ZVS energy of the switch $Q_1$, and the ZVS condition of $Q_1$ is improved. Fig. 10 shows the maximum $L_m$ required for the ZVS of $Q_1$ under the same $L_{lkg}$ with 15 $\mu$H. To achieve the ZVS under the same load conditions, the conventional AHB converter should be designed with a small $L_m$ of 400 $\mu$H, whereas the proposed converter can be designed with a relatively large $L_m$ of 900 $\mu$H. Although it is designed with a larger $L_m$, it can achieve the ZVS of $Q_1$ well enough. As a result, $Q_1$ turns ON after more of the voltages of output capacitance $C_{oss}$ are discharged under light-load conditions, which results in mitigated turn-ON switching loss.

### D. Primary RMS Current

The primary rms current can be determined in Fig. 3. To ease the complexity of analysis, it is assumed that the dead time [$t_3$-$t_4$] is small enough to be neglected. At this time, the primary current corresponding to each time is obtained as follows:

$$\begin{aligned} i(t_0) &= I_{Lm\_offset} - \tfrac{1}{2}\cdot\Delta i_{Lm} + \tfrac{I_O}{n} \\ i(t_1) &= I_{Lm\_offset} + \tfrac{1}{2}\cdot\Delta i_{Lm} + \tfrac{I_O}{n} \\ i(t_2) &= I_{Lm\_offset} + \tfrac{1}{2}\cdot\Delta i_{Lm} - \tfrac{I_O}{n} \\ i(t_3) &= I_{Lm\_offset} - \tfrac{1}{2}\cdot\Delta i_{Lm} - \tfrac{I_O}{n} \end{aligned} \quad (16)$$

where $I_{Lm\_offset}$ is the dc offset of magnetizing current, and $\Delta i_{Lm}$ is a ripple of magnetizing current.

From (16), the primary rms current of the conventional AHB converter and the proposed converter are, respectively, obtained as follows:

$$i_{lkg\_RMS\_Conv} = \left[\frac{1}{T}\{\int_0^{DT_S}\left(\frac{\Delta i_{Lm}}{DT_S}t+i(t_0)\right)^2dt + \int_0^{(1-D)T_S}\left(\frac{-\Delta i_{Lm}}{(1-D)T_S}t+i(t_2)\right)^2dt\}\right]^{\frac{1}{2}} \quad (17)$$

$$i_{lkg\_RMS\_Prop} = \left[\frac{1}{T}\left\{\int_0^{DT_S}\left(\frac{\Delta i_{Lm}}{DT_S}t+i(t_0)\right)^2dt + \int_0^{(1-2D)T_S}\left(\frac{-2I_O/n}{(1-2D)T_S}t+i(t_1)\right)^2dt + \int_0^{DT_S}\left(\frac{-\Delta i_{Lm}}{DT_S}t+i(t_2)\right)^2dt\}\right]^{\frac{1}{2}}. \quad (18)$$

Fig. 11 shows the primary rms current of the conventional AHB converter with $L_m$ of 400 $\mu$H and the proposed converter with $L_m$ of 900 $\mu$H. Due to the symmetrical operation and large $L_m$, the proposed converter has a smaller primary rms current than the conventional AHB converter. In addition, it can be designed as a small size of the transformer due to the zero dc offset of magnetizing current. Although the proposed converter has a slightly increased primary turn $N_P$ of winding than the conventional AHB converter, it has a small mean-length per turn of the winding due to the small size of the transformer. As a result, the proposed converter has 1.18 W smaller conduction loss of the transformer than the conventional AHB converter.

### E. Transformer Design

To select the appropriate transformer core, $A_P$ value is widely used. The $A_P$ value is as follows:

$$A_P = \frac{L_mI_{Lm\_max}}{B_{max}K_uJ}\left(i_{pri\_RMS}+\frac{i_{sec\_RMS}}{n}\right) \quad (19)$$

where $L_m$ is the magnetizing inductance, $I_{Lm\_max}$ is the maximum magnetizing current, $N_P$ is the primary turn of winding, $B_{max}$ is the maximum flux density, $K_u$ is the utilization factor,

$J$ is the current density, $i_{\mathrm{pri\cdot RMS}}$ is the primary rms current, and $i_{\mathrm{sec\cdot RMS}}$ is the secondary rms current.

The proposed converter does not have a dc offset of magnetizing current, which results in small $I_{Lm\cdot\max}$. Under the same $B_{\max}$, $K_u$, and $J$, $A_P$ value of the proposed converter is about 17574 mm$^4$ through (19). Consequently, the transformer core of the proposed converter was selected as PQ3230, which is 6160.2 mm$^3$ smaller in volume than the conventional AHB converter.

### *F. Comparison of Output Inductor Between the AHB Converter With the CIR and Proposed Converter*

To obtain the symmetrical operation, as shown in Fig. 7, an additional voltage source is required to reduce $v_{lkg}$ in the commutation. Accordingly, the proposed converter uses a capacitor instead of a coupled inductor presented in [21] as the voltage source.

As shown in Fig. 2(b), the offset current of the coupled inductor is twice the $I_O$ because the AHB converter with the CIR is derived from the voltage doubler rectifier. Hence, the rms current of the coupled inductor is large, as shown in (20), and large conduction loss occurs

$$i_{Lo\_\mathrm{CIR\_RMS}} = 2I_O\sqrt{\frac{D+1}{3}}. \tag{20}$$

Meanwhile, since the proposed converter has the offset current of $L_O$ as $I_O$, the rms current of $L_O$ is small as in (21).

$$i_{Lo\_\mathrm{Prop\_RMS}} = I_O. \tag{21}$$

The proposed converter has 4.74 W smaller conduction loss of output inductor due to the smaller rms current and smaller size of the output inductor than the AHB converter with CIR. Consequently, the proposed converter is more advantageous in terms of the conduction loss of output inductor than the AHB converter with the CIR.

### *G. Output Inductor Design*

The output inductor is designed in order for the ripple condition of output current to satisfy peak-to-peak 20%. The output inductance is determined by the voltage and current ripple applied to the output inductor based on the following:

$$L_O = \frac{V_{LO}\cdot\Delta t}{\Delta i_{Lo}} \tag{22}$$

where $V_{LO}$ is the voltage of the output inductor and $\Delta i_{LO}$ is the ripple current of the output inductor.

Fig. 12 shows the output inductance based on (22). $L_O$ values of the conventional AHB converter, AHB converter with CIR, and the proposed converter under given conditions are 120 $\mu$H, 60 $\mu$H, and 240 $\mu$H, respectively. To design the appropriate output inductor core, $A_P$ value as in (19) is widely used, similar to a transformer. Under the same $B_{\max}$, $K_u$, and $J$, the $A_P$ values of the proposed converter is 9251 mm$^4$. As a result, since the proposed converter has a small offset current of the output inductor and small rms current of the output inductor, the output inductor of the proposed converter is designed as CH270060, which is 1332.8 mm$^3$ smaller in volume than the AHB converter with CIR.

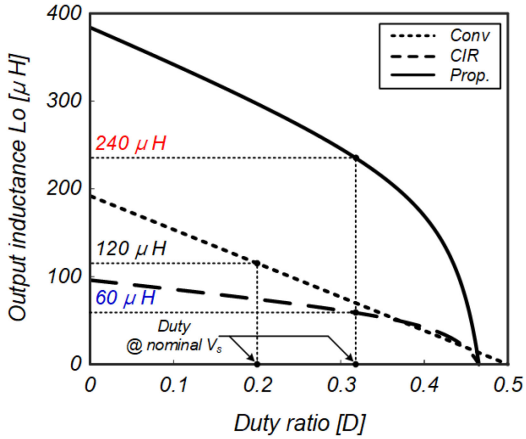


Fig. 12. Design results of output inductance.

### *H. Voltage Stress and Average Current of Diode*

As shown in Fig. 6, the voltage stresses of diodes $D_1$, $D_2$, $D_3$, and $D_4$ in the proposed converter are obtained as follows:

$$v_{D1} = v_{D4} = -v_{rec} - V_{CS} = \frac{2I_O L_{lkg}}{n^2(1-2D)T_S} \tag{23}$$

$$v_{D2} = v_{D3} = v_{rec} + V_{CS} = \frac{V_S}{n} - \frac{2I_O L_{lkg}}{n^2(1-2D)T_S}. \tag{24}$$

If the operating duty ratio is less than 0.5, the voltage stress of $D_2$ and $D_3$ is higher than that of $D_1$ and $D_4$. Thus, the aforementioned AHB converters have asymmetrical voltage stress of diode. For diodes with low voltage stress, $v_{D1}$ and $v_{D4}$ of the proposed converter are the same as the AHB converter with the CIR and are slightly lower than that of the conventional AHB converter. For diodes with high voltage stress, $v_{D2}$ and $v_{D3}$ of the proposed converter are the same as the AHB converter with the CIR and are slightly higher than that of the conventional AHB converter.

In the design of a diode, current stress as well as voltage stress must be considered. The conventional AHB converter has the average currents in $D_2$ and $D_3$ of $(1-D)I_o$ and the average currents in $D_1$ and $D_4$ of $DI_o$. Thus, the conventional AHB converter has an unbalanced average current of diodes. Meanwhile, the AHB converter with the CIR and the proposed converter have the average currents in all rectifier diodes of $I_o$ and $0.5I_o$, respectively. Thus, they have a balanced average current regardless of voltage stress. Although the aforementioned converters are designed with the same rated voltage of the diode, the proposed converter can be designed as a diode with a low current rating due to its low average current. As a result, $D_1$ and $D_4$ were selected as 150-V-rated diodes with low current rating, and $D_2$ and $D_3$ were selected as 400-V-rated diodes with low current rating.

In general, diodes with high voltage stress have high $V_F$. Therefore, since the high average current flows through the diodes with high voltage stress, the conventional AHB converter has a large conduction loss of diode. However, the AHB converter with CIR and the proposed converter have a smaller conduction loss of diode than the conventional AHB converter due to the balanced average currents. In addition, the proposed

TABLE II
DESIGN PARAMETER FOR AN EXPERIMENT

| | *AHB converter* | *AHB converter with CIR* [21] | *Proposed AHB converter* |
|---|---|---|---|
| Primary switch $Q_1$, $Q_2$ | IPP60R280P7 (600 *V*, 280 *mΩ*) | | |
| Transformer | *PQ3530 (400 μH, 44:19)* | *PQ3230 (900 μH, 46:9)* | *PQ3230 (900 μH, 46:18)* |
| Leakage inductance | *15 μH* | | |
| ZVS range of $Q_1$ | *50% load conditions* | | |
| Rectifier Diode $D_1$ *and* $D_4$ | *STPS10150CT * 2ea (150 V, 10 A, 0.8 $V_F$)* | *STPS20150CT (150 V, 20 A, 0.84 $V_F$)* | *STPS10150CT * 2ea (150 V, 10 A, 0.8 $V_F$)* |
| Rectifier Diode $D_2$ *and* $D_3$ | *MUR1540G * 2ea (400 V, 15 A, 1 $V_F$)* | *MUR1540G (400 V, 15 A, 1 $V_F$)* | *MUR840G * 2ea (400 V, 8 A, 0.9 $V_F$)* |
| RCD Snubber of $D_1$ *and* $D_4$ | *22 kΩ* | *55 kΩ* | *55 kΩ* |
| RCD Snubber of $D_2$ *and* $D_3$ | *67.1 kΩ* | *64.8 kΩ* | *67.6 kΩ* |
| Rectifier capacitor $C_S$ | - | *Ceramic capacitor (100 V, 10 μF) * 4ea* | *Ceramic capacitor (100 V, 10 μF) * 2ea* |
| Output inductor $L_O$ | *CH234060 (120 μH, 47)* | *CH330060 (60 μH, 35:35)* | *CH270060 (240 μH, 60)* |
| Output capacitor $C_O$ | *Aluminum electrolytic capacitor (100 V, 270 μF) * 1ea* | | |
| Total volume | *37 379.4 $mm^3$* | *33 593.8 $mm^3$* | *33 131 $mm^3$* |

converter can use lower current-rating diodes than the AHB converter with the CIR. Therefore, $V_F$ and reverse recovery characteristics of the diodes are improved. Consequently, the proposed converter has advantages in terms of conduction loss and characteristics of diodes.

### I. Design of Secondary Capacitor

Since the secondary capacitor acts as a voltage source, the voltage ripple condition is designed to satisfy the peak-to-peak 5%. The voltage $V_{CS}$ and voltage ripple of the secondary capacitor are equal to (7) and (25), respectively

$$\Delta V = \frac{T_S \cdot \Delta I_{CS}}{8C_S} + \Delta I_{CS} \cdot \mathrm{ESR} \tag{25}$$

where $\Delta I_{CS}$ is the current ripple of the secondary capacitor, $C_S$ is the secondary capacitance, and ESR is the equivalent series resistance of the capacitor.

Based on (7), since $V_{CS}$ has a maximum value at the nominal input voltage, $V_{CS\cdot\max}$ is approximately 48 V, which is the output voltage. In addition, the voltage ripple is composed of the effect of ESR and the charge/discharge of the capacitor, as shown in (25). Therefore, $C_S$ was selected as 20 $\mu$F under the given conditions using (25). Moreover, the current ripple condition must be considered because self-heating occurs due to the current flowing through the capacitor. As a result, considering that $V_{CS\cdot\max}$ is 48 V and $\Delta I_{CS}$ is $2I_O$, $C_S$ is selected to two CKG57KX7S2A106K335JJ (10 $\mu$F, 100 V) in parallel.

## V. EXPERIMENTAL RESULTS

The effectiveness and feasibility of the proposed converter were verified with the experimental results. The design specification is 300–400 V input voltage, 48 V/400 W output, and 100 kHz switching frequency. For comparison, the conventional AHB converter and the AHB converter with the CIR were also implemented. The design parameters for an experiment are listed in Table II. The primary-side configuration and control of the aforementioned AHB converters are identical. As shown in Table II, the AHB converter with the CIR and the proposed converter can be designed with a small size transformer due to zero dc offset of magnetizing current. In addition, they can be designed with a larger $L_m$ because the ZVS condition of $Q_1$ is improved. $L_O$ is designed so that the current ripple of the output capacitor is the same. Moreover, the resistor-capacitor-diode (RCD) snubber is designed so that the voltage ringing of the diode is clamped at a similar voltage level.

Fig. 13 shows the experimental setup. To verify the feasibility of the proposed converter, a Sorensen SGA600/17C-0AAA was used as the input source, and series–parallel connected electric loads (Prodigit 3353) were used as output loads. The efficiency was measured with a Yokogawa WT3000, and the waveforms were observed using Teledyne Lecroy HDO8038 and WaveRunner8054.

Fig. 14 shows the prototype of the aforementioned converters. As shown in Fig. 14, the magnetic component has the greatest influence on the size of the converter. For the transformer, the AHB converter with CIR and the proposed converter have a transformer with a smaller volume of 6160.2 $mm^3$ due to the zero dc offset of magnetizing current. For the output inductor, the proposed converter has an output inductor with a smaller

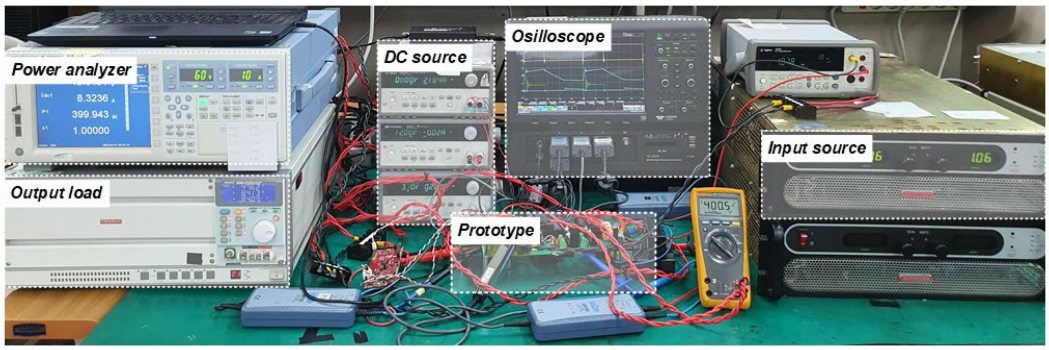


Fig. 13. Photograph of the experimental setup.

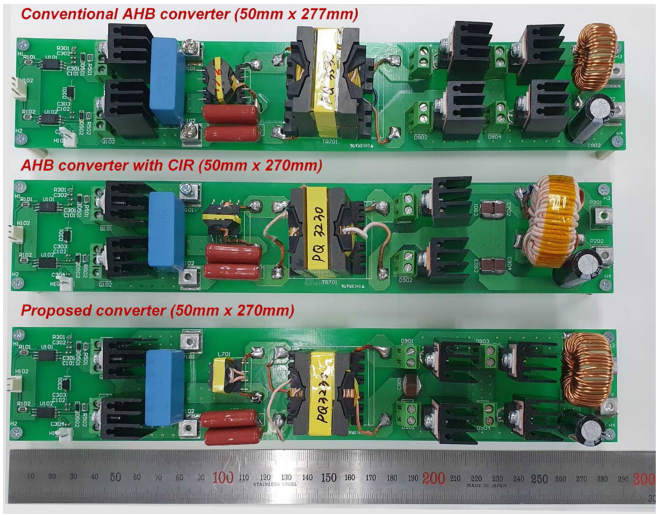


Fig. 14. Photograph of the prototype converters.

volume of 1332.8 mm$^3$ than the AHB converter with CIR, while it has a output inductor with a larger volume of 1872.6 mm$^3$ than the conventional AHB converter. Therefore, when comparing the volume of the diode and the added secondary capacitor as well as the magnetic component, the total volumes of the conventional AHB converter, AHB converter with CIR, and proposed converter are 37379.4 mm$^3$, 33593.8 mm$^3$, and 33131 mm$^3$, respectively. In conclusion, the proposed converter has the smallest size of the prototype, as shown in Fig. 14.

Fig. 15 shows the experimental waveforms at nominal input voltage under 100% load conditions. As shown in Fig. 15(a), the conventional AHB converter operates at a low duty ratio of 0.22 due to the nonlinear voltage gain and performs the asymmetrical operation. Hence, it has a dc offset of magnetizing current. As shown in Fig. 15(b), the AHB converter with the CIR operates with a relatively high duty ratio of 0.34 by linear voltage gain. The coupled inductor serves as the voltage source in the commutation period to perform the symmetrical operation. Hence, it has a zero dc offset of magnetizing current. As shown in Fig. 15(c), the proposed converter operates the same as the AHB converter with the CIR. Similarly, it operates at a relatively high duty ratio of 0.34 by a linear voltage gain. In addition, it performs the symmetrical operation as the secondary capacitor serves as the voltage source in the commutation period. Hence, it has a zero dc offset of magnetizing current. Furthermore, the aforementioned AHB converters have asymmetrical voltage stress of diode at a nominal input voltage. Therefore, different RCD snubbers were used to limit the secondary-side voltage ringing according to the voltage stress, and it can be seen that the diode with high voltage stress is clamped at 360 V.

Fig. 16 shows the ZVS waveforms of $Q_1$ at nominal input voltage with different load conditions. As shown in Fig. 16(a) and (b), the conventional AHB converter has the small ZVS energy of $Q_1$ due to the dc offset of magnetizing current. Thus, it can achieve the ZVS under 50% load conditions with small $L_m$. However, hard switching occurs at 400 V under 10% load conditions. As shown in Fig. 16(c)–(f), the AHB converter with the CIR and the proposed converter have the same ZVS characteristics because they have the same primary operation. In addition, the ZVS energy of $Q_1$ is large due to the zero dc offset of magnetizing current. Thus, they can achieve the ZVS under 50% load conditions as the conventional AHB converter, even with a large $L_m$. Moreover, hard switching occurs at 390 V after discharging the voltage of $Q_1$ more than the conventional AHB converter under 10% load conditions. Therefore, the proposed converter has mitigated the turn-ON switching loss under light-load conditions.

Figs. 17 and 18 show the measured efficiency of the prototype converters and the loss breakdown at a nominal input voltage. As shown in Fig. 17, the proposed converter achieves higher efficiency under entire load conditions than the conventional AHB converter and the AHB converter with the CIR. Based on the loss breakdown, as shown in Fig. 18, it has a higher efficiency than the conventional AHB converter due to small switching loss under light-load conditions and small conduction loss of the transformer and diode under heavy-load conditions. In addition, it has a higher efficiency than the AHB converter with the CIR due to the reduced conduction loss of the output inductor and diode under heavy-load conditions.

## VI. Conclusion

In this article, an AHB converter with linear voltage gain is proposed. The proposed converter has a structure in which a secondary capacitor is added for the extended commutation period. It has the following advantages through linear voltage gain and

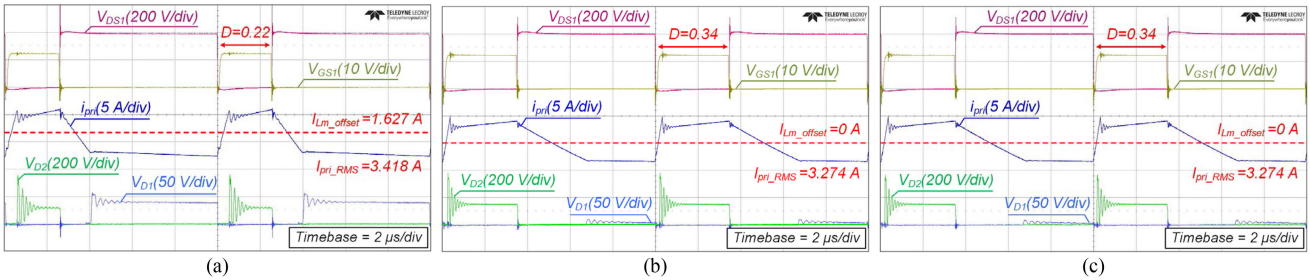


Fig. 15. Experimental waveforms under 100% load conditions. (a) Conventional AHB converter. (b) AHB converter with the CIR. (c) Proposed converter.

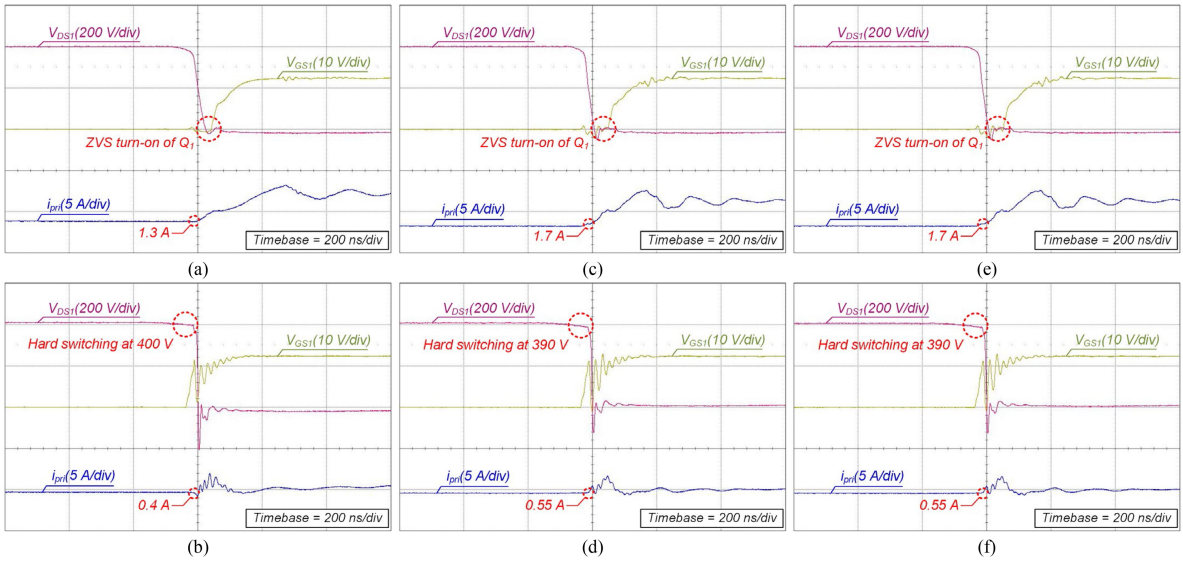


Fig. 16. Experimental ZVS waveforms. (a) Conventional AHB converter under 50% load conditions. (b) Conventional AHB converter under 10% load conditions. (c) AHB converter with the CIR under 50% load conditions. (d) AHB converter with the CIR under 10% load conditions. (e) Proposed converter under 50% load conditions. (f) Proposed converter under 10% load conditions.

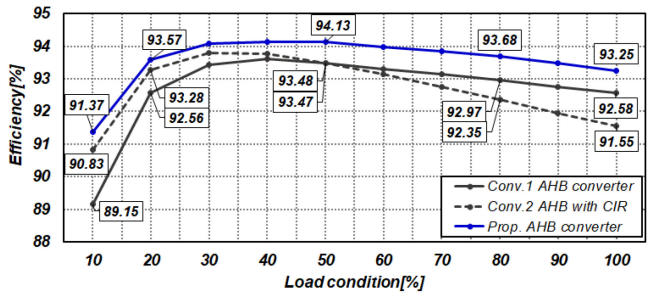


Fig. 17. Measured efficiency at nominal input voltage.

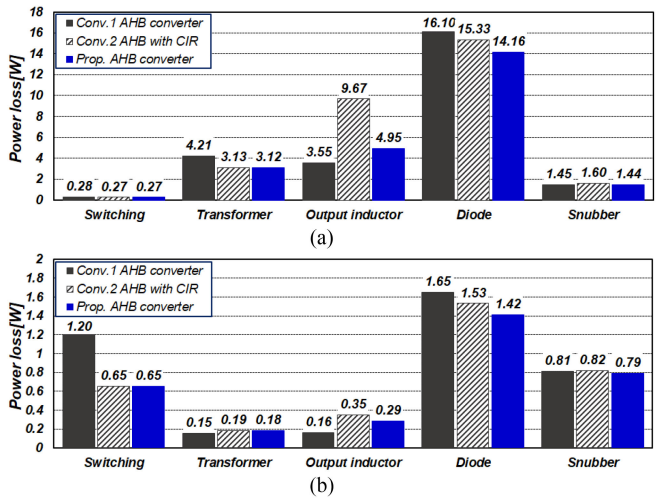


Fig. 18. Loss breakdown of prototype at nominal input voltage. (a) 100% load conditions. (b) 10% load conditions.

symmetrical operation. First, it has a narrow range of operating duty ratio by linear voltage gain. Second, it has a zero dc offset of magnetizing current that reduces the size of the transformer. Besides, zero dc offset of magnetizing current affects primary current to operate symmetrically, which results in large ZVS energy of $Q_1$. Therefore, it has a reduced switching loss because the ZVS condition of $Q_1$ is improved. In addition, it has reduced conduction loss due to low primary rms current through large $L_m$ and balanced average current of the diode. Furthermore, since it can use lower current-rating diodes, the characteristics of diodes are improved. Consequently, the proposed converter is suitable for low to medium power applications with a 48 V system as an alternative to the conventional AHB converter.

## REFERENCES


[1] C. Lin, O. Song, and J. Wang, "A new high efficiency and high power density 48V to 1V converter," in *Proc. IEEE 1st Int. Power Electron. Appl. Symp.*, 2021, pp. 1–3.

[2] I.-H. Cho, K.-M. Cho, J.-W. Kim, and G.-W. Moon, "A new phase-shifted full-bridge converter with maximum duty operation for server power system," *IEEE Trans. Power Electron.*, vol. 26, no. 12, pp. 3491–3500, Dec. 2011.

[3] W. Li, Y. He, X. He, Y. Sun, F. Wang, and L. Ma, "Series asymmetrical half-bridge converters with voltage autobalance for high input-voltage applications," *IEEE Trans. Power Electron.*, vol. 28, no. 8, pp. 3665–3674, Aug. 2013.

[4] X. Xu, A. M. Khambadkone, T. M. Leong, and R. Oruganti, "A 1-MHz zero-voltage-switching asymmetrical half-bridge DC/DC converter: Analysis and design," *IEEE Trans. Power Electron.*, vol. 21, no. 1, pp. 105–113, Jan. 2006.

[5] M. Arias, M. F. Diaz, D. G. Lamar, F. M. F. Linera, and J. Sebastián, "Small-signal and large-signal analysis of the two-transformer asymmetrical half-bridge converter operating in continuous conduction mode," *IEEE Trans. Power Electron.*, vol. 29, no. 7, pp. 3547–3562, Jul. 2014.

[6] T. Mishima and M. Nakaoka, "A novel high-frequency transformer-linked soft-switching half-bridge DC–DC converter with constant-frequency asymmetrical PWM scheme," *IEEE Trans. Ind. Electron.*, vol. 56, no. 8, pp. 2961–2969, Aug. 2009.

[7] P. Imbertson and N. Mohan, "Asymmetrical duty cycle permits zero switching loss in PWM circuits with no conduction loss penalty," *IEEE Trans. Ind. Appl.*, vol. 29, no. 1, pp. 121–125, Jan./Feb. 1993.

[8] R. Oruganti, P. C. Heng, J. T. K. Guan, and L. A. Choy, "Soft-switched DC/DC converter with PWM control," *IEEE Trans. Power Electron.*, vol. 13, no. 1, pp. 102–114, Jan. 1998.

[9] I.-O. Lee and G.-W. Moon, "A new asymmetrical half-bridge converter with zero DC-offset current in transformer," *IEEE Trans. Power Electron.*, vol. 28, no. 5, pp. 2297–2306, May 2013.

[10] P. Moo-Hyun, C.-O. Yeon, J.-S. Park, C.-Y. Lim, J.-K. Han, and G.-W. Moon, "Wide-range ZVS asymmetric half-bridge converter with clamping switches for small DC offset current," in *Proc. IEEE 8th Int. Power Electron. Motion Control Conf*., 2016, pp. 2262–2269.

[11] M. Arias, D. G. Lamar, F. F. Linera, D. Balocco, A. Aguissa Diallo, and J. Sebastián, "Design of a soft-switching asymmetrical half-bridge converter as second stage of an LED driver for street lighting application," *IEEE Trans. Power Electron.*, vol. 27, no. 3, pp. 1608–1621, Mar. 2012.

[12] B.-R. Lin and C.-H. Tseng, "Analysis of parallel-connected asymmetrical soft-switching converter," *IEEE Trans. Ind. Electron.*, vol. 54, no. 3, pp. 1642–1653, Jun. 2007.

[13] S. Chakraborty and S. Chattopadhyay, "An improved asymmetric half-bridge converter with zero DC offset of magnetizing current," in *Proc. IEEE Appl. Power Electron. Conf. Expo.*, 2015, pp. 1–8.

[14] W. Eberle and Y.-F. Liu, "A zero voltage switching asymmetrical half-bridge DC/DC converter with unbalanced secondary windings for improved bandwidth," in *Proc. IEEE 33rd Annu. IEEE Power Electron. Specialists Conf*., 2002, vol. 4, pp. 1829–1834.

[15] C.-O. Yeon, J.-B. Lee, I.-O. Lee, and G.-W. Moon, "Wide ZVS range asymmetric half-bridge converter with clamp switch and diode for high conversion efficiency," *IEEE Trans. Ind. Electron.*, vol. 63, no. 5, pp. 2862–2870, May 2016.

[16] K.-M. Cho, W.-S. Oh, K.-W. Lee, and G.-W. Moon, "A new half bridge converter for the personal computer power supply," *Proc. IEEE Power Electron. Specialists Conf*., 2008, pp. 986–991.

[17] J.-K. Han, J.-W. Kim, and G.-W. Moon, "A high-efficiency asymmetrical half-bridge converter with integrated boost converter in secondary rectifier," *IEEE Trans. Power Electron.*, vol. 32, no. 11, pp. 8237–8242, Nov. 2017.

[18] H. Mao, J. Abu-Qahouq, S. Luo, and I. Batarseh, "Zero-voltage-switching half-bridge DC-DC converter with modified PWM control method," *IEEE Trans. Power Electron.*, vol. 19, no. 4, pp. 947–958, Jul. 2004.

[19] J.-B. Lee, J.-K. Kim, J.-H. Kim, J.-I. Baek, and G.-W. Moon, "A high-efficiency PFM half-bridge converter utilizing a half-bridge LLC converter under light load conditions," *IEEE Trans. Power Electron.*, vol. 30, no. 9, pp. 4931–4942, Sep. 2015.

[20] J.-I. Baek, J.-K. Kim, J.-B. Lee, H.-S. Youn, and G.-W. Moon, "Integrated asymmetrical half-bridge zeta (AHBZ) converter for DC/DC stage of LED driver with wide output voltage range and low output current," *IEEE Trans. Ind. Electron.*, vol. 62, no. 12, pp. 7489–7498, Dec. 2015.

[21] J.-K. Han, J.-W. Kim, B.-H. Lee, J.-S. Lai, and G.-W. Moon, "High-efficiency asymmetrical half-bridge converter with a new coupled inductor rectifier (CIR)," *IEEE Trans. Power Electron.*, vol. 34, no. 12, pp. 11541–11552, Dec. 2019.


**Juhyun Bae** (Student Member, IEEE) received the B.S. degree in electrical engineering in 2020 from Hanyang University, Seoul, South Korea, and the M.S. degree in electrical engineering in 2022 from the Korea Advanced Institute of Science and Technology, Daejeon, South Korea, where he is currently working toward the Ph.D. degree in electrical engineering.

His main research interests include high efficiency dc–dc converter and battery management system.

**Jae-Sang Kim** (Student Member, IEEE) received the B.S. degree in electrical engineering from Hanyang University, Seoul, South Korea, in 2018, and the M.S. degree in electrical engineering in 2020 from the Korea Advanced Institute of Science and Technology, Daejeon, South Korea, where he is currently working toward the Ph.D. degree in electrical engineering.

His main research interests include the design and control of dc/dc converters, and high-frequency power converters (based on a document published on September 21, 2020).

**Minsu Lee** (Student Member, IEEE) received the B.S. degree in electrical engineering in 2017 from the Korea Advanced Institute of Science and Technology, Daejeon, South Korea, where he is currently working toward the Ph.D. degree in electrical engineering.

His research interests include high-efficiency dc/dc converter topology, electric vehicle charger system, server power system, dc microgrid, converter topologies, and magnetics.

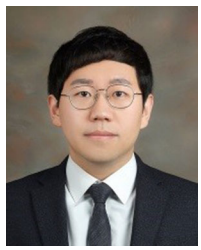

**Jung-Kyu Han** (Member, IEEE) was born in South Korea, in 1991. He received the B.S., M.S., and Ph.D. degrees in electrical engineering from the Korea Advanced Institute of Science and Technology (KAIST), Daejeon, Korea, in 2014, 2016, and 2020, respectively. He was awarded a highlighted paper in IEEE Transactions on Power Electronics in 2019, and he presented a webinar in the IEEE Power Electronics Society and IEEE PELS and IES Bangalore Section in 2020.

From 2020 to 2022, he worked as a research engineer in the Samsung Electronics R&D center. Since 2022, he has been working as an Assistant Professor in the Department of Electronics and Control Engineering, Hanbat National University, Daejeon, Korea. His research interests include dc-dc converters, PFC converters, digital control, on-board charger for EV, and 27.12 MHz power amplifier.

**Gun-Woo Moon** (Member, IEEE) received the M.S. and Ph.D. degrees in electrical engineering from the Korea Advanced Institute of Science and Technology (KAIST), Daejeon, South Korea, in 1992 and 1996, respectively.

He is currently a Professor with the Department of Electrical Engineering, KAIST, Daejeon. His research interests include modeling, design, and control of power converters, soft-switching power converters, resonant inverters, distributed power systems, power-factor correction, electric drive systems, driver circuits of plasma display panels, and flexible ac transmission systems.

Dr. Moon is a member of the Korean Institute of Power Electronics, the Korean Institute of Electrical Engineers, the Korea Institute of Telematics and Electronics, the Korea Institute of Illumination Electronics and Industrial Equipment, and the Society for Information Display.